

FUNDAMENTAL STUDIES OF NEURAL STIMULATING ELECTRODES

Sixth Quarterly Report
Covering Period November 29, 1995 to February 28, 1996
CONTRACT NO. N01-NS-4-2310

T. L. Rose
S. F. Cogan
L. S. Robblee
U. M. Twardoch
G. S. Jones
R. B. Jones

EIC Laboratories, Inc.
111 Downey Street
Norwood, Massachusetts 02062

Prepared for

National Institutes of Health
National Institute of Neurological
Disorders and Stroke
Bethesda, Maryland 20892

April, 1996

This QPR is being sent to
you before it has been
reviewed by the staff of the
Neural Prosthesis Program.

TABLE OF CONTENTS

<u>Section</u>	<u>Page</u>
1. INTRODUCTION AND SUMMARY.....	5
2. VOLTAMMETRY STUDIES ON Ir MICROELECTRODE.....	7
2.1. Modifications of Test Cell.....	7
2.2. U. Michigan Ribbon-Cable Probe 1, site 1.....	9
2.3. U. Michigan Ribbon-Cable Probe 2, site 5.....	15
3. ELECTROCHEMICAL IMPEDANCE SPECTROSCOPY.....	24
3.1. Experimental Protocol for EIS Measurements.....	24
3.2. Three-Dimensional Plots of EIS Data.....	27
3.3. Circuit Analysis of the EIS Data.....	31
4. WORK FOR NEXT QUARTER.....	33
5. REFERENCES.....	35

LIST OF FIGURES

	<u>Page</u>
Figure 2.1 Schematic representation of U. Michigan ribbon-cable probe and numbering scheme for the electrode sites.....	7
Figure 2.2 Schematic diagram of lid for test cell used for electrochemical measurements of the U. Michigan ribbon-cable probes.....	8
Figure 2.3 Comparison of apparent capacitance of site 1 on U. Michigan ribbon-cable probe No. 1 calculated from the currents in Table 2.1 for the ten scan rate studies.....	11
Figure 2.4 Comparison of the cyclic voltammograms of site 1 on U. Michigan ribbon cable-probe No. 1 acquired on day 35 (left) and day 108 (right).....	13
Figure 2.5 Comparison of voltammograms over a wide potential range to evaluate oxide growth on U. Michigan ribbon cable-probe No. 1 site 1 acquired on day 34 (solid line) and day 113 (broken line).....	14
Figure 2.6 Cyclic voltammograms of the six sites on the U. Michigan ribbon-cable probe No. 2 in non-deaerated 0.1 M PBS at 0.05 V/s before and after the scan rate study on site 5.....	16
Figure 2.7 Cyclic voltammograms of site 5 of U. Michigan ribbon-Cable probe No. 2 before (solid line) and after (broken line) Ru hexaamine portion of the scan rate study	18
Figure 3.1 (a) Cyclic voltammograms of site 2 of U. Michigan ribbon-cable probe No. 4 before the first EIS measurement, and before and after the second EIS measurement. (b) Cyclic voltammograms of site 1 of U. Michigan ribbon-cable probe No. 1 before and after the EIS measurement.....	26
Figure 3.2 Three-dimensional Bode plots of EIS (study 2) of site-2 of U. Michigan ribbon cable No. 4 taken in deaerated PBS.....	28
Figure 3.3 Three-dimensional Bode plots of EIS (study 1) of site-2 of U. Michigan ribbon-cable No. 4 taken in partially deaerated PBS.....	29
Figure 3.4 Three-dimensional Bode plots of EIS (study 1) of site-1 of U. Michigan ribbon cable No. 1 taken in aerated PBS after completion of Ru scan rate study	30
Figure 3.5 Comparison of the magnitude of the impedance as a function of electrode bias at three frequencies for the three EIS measurements.....	32

LIST OF TABLES

	<u>Page</u>
Table 2.1 Current measurements for the ten scan rate studies on site 1 of U. Michigan ribbon-cable probe No. 1.....	10
Table 2.2 Dimensions of site 1 on U. Michigan ribbon-cable probe No. 1.....	12
Table 2.3 Data for electrochemical study 1 on site 5 of U. Michigan ribbon-cable probe No. 2.....	19
Table 2.4 Comparison of electrochemical testing of U. Michigan sputtered film and HMRI wire microelectrodes.	22
Table 3.1 Electrodes characterized with EIS	26

1. INTRODUCTION AND SUMMARY

This report describes the work on NINDS Contract No. N01-NS-4-2310 during the period November 29, 1995 to February 28, 1996. As part of the Neural Prosthesis Program, the broad objectives of the present fundamental studies are: 1) to evaluate the electrochemical processes that occur at the electrode-electrolyte interface during pulsing regimens characteristic of neural prosthetic applications; 2) to establish charge injection limits of stimulation electrode materials which avoid irreversible electrochemical reactions; 3) to develop an *in vitro* method, which can be applied *in vivo*, for determining the electrochemical real area and stability of microelectrodes; 4) to develop new materials which can operate at high stimulation charge densities for microstimulation; and 5) to provide electrochemical and analytical support for other research activities in the Neural Prosthesis Program at NINDS.

Long term stability studies of a U. Michigan ribbon cable-probe which were initiated in the fifth quarter were continued. After remaining nearly constant for the first 76 days of soaking in 0.1 M PBS, the electrochemically active surface area of the Ir microelectrode increased fivefold based on the apparent capacitance at high sweep rates. The cyclic voltammograms also showed increasing current in the symmetrical peaks representative of oxide growth even though the electrode was not intentionally activated.

Studies were initiated this quarter to determine the cause of the "activation" of the Ir microelectrodes during our testing procedures because this activation prohibits quantitative analysis of the geometric properties of the electrodes by the Ru technique. Cyclic voltammograms in aerated PBS were taken prior to the Ru scan rate study on one site of a ribbon-cable probe. During these sweeps some activation occurred despite restricting the potential limits to values that are generally not expected to lead to oxide growth. Because of this oxide growth, corrections for the background current to the data from the scan rate studies utilizing mass transport of Ru hexaammine could not be made for the higher sweep rates.

Further modifications were made in the design of the lid of the cell to test the ribbon cable electrodes under conditions which rigorously excluded oxygen. Electrochemical impedance spectroscopy (EIS) was run on one site of a new ribbon cable probe to determine if

any activation occurred during these measurements. The results based on the CV of the site before and after EIS showed that very little activation had occurred.

The EIS of the unactivated Ir site on the ribbon cable was made in a deaerated PBS solution and a solution with some oxygen present. A principle feature of the EIS data is the decrease in the impedance of the electrode at low frequencies and negative bias when oxygen is present. This response is consistent with the reduction of oxygen on the electrode. The initial attempts were made to fit the EIS data to an electronic circuit diagram. Preliminary results show that measurements at sufficiently high frequency may be useful to separate the double layer capacitance of the Ir metal surface from the capacitance of the oxide on the film.

The electrochemical characterization studies of the ribbon electrode in the new, improved, air-tight cell will be continued in the next quarter and expanded to include purposefully activated Ir sites. The studies will include cyclic voltammetry, EIS, and pulse stimulation. We will also begin evaluating Ru/Ir mixed oxide as a possible electrode material for high density charge stimulation or a material with enhanced stability under pulse conditions.

2. VOLTAMMETRY STUDIES ON Ir MICROELECTRODE

During this quarter we continued studies of the long term stability of Ir sites on a probe with an integrated ribbon cable received from U. Michigan. We also evaluated the electrochemical surface area of an additional ribbon-cable probe under modified conditions. A third probe was monitored for site integrity using a combination of cyclic voltammetry and impedance spectroscopy. The integrated ribbon cables allow long term soaking studies without any structures other than those fabricated on the wafer being exposed to the electrolyte solution which avoids the previous problems with electrolyte penetration beneath the epoxy covering the contact pads. Figure 2.1 is a diagrammatic representation of the probe showing the numbering scheme for the electrode sites.

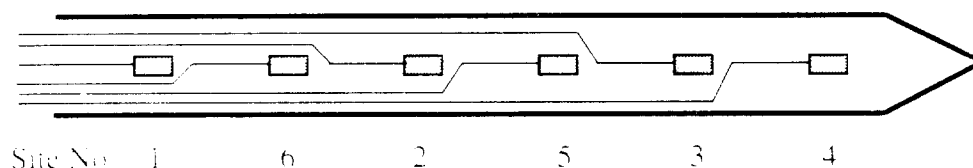


Figure 2.1 Schematic representation of U. Michigan ribbon-cable probe and numbering scheme for the electrode sites.

2.1. Modifications of Test Cell.

Last quarter a cell assembly was fabricated to hold a ribbon-cable probe semi-permanently at a fixed position in the cell. The lid of the assembly was modified this quarter to enhance the ability to deaerate the solution and exclude air from entering the cell during the quiescent electrochemical testing. Figure 2.2 is a schematic diagram of the lid and assembled system. The reference and counter electrodes are fitted tightly into the lid. The purging gas inlet and exhaust are connected to an argon tank and gas bubbler, respectively. The ribbon cable of the probe is sealed with dental wax in a capillary tube which extends into the cell. The tube prevents the ribbon from flexing too much in the solution and protects the probe from inadvertent contact with the other components in the cell. The Microdot receptacle for the plug attached to

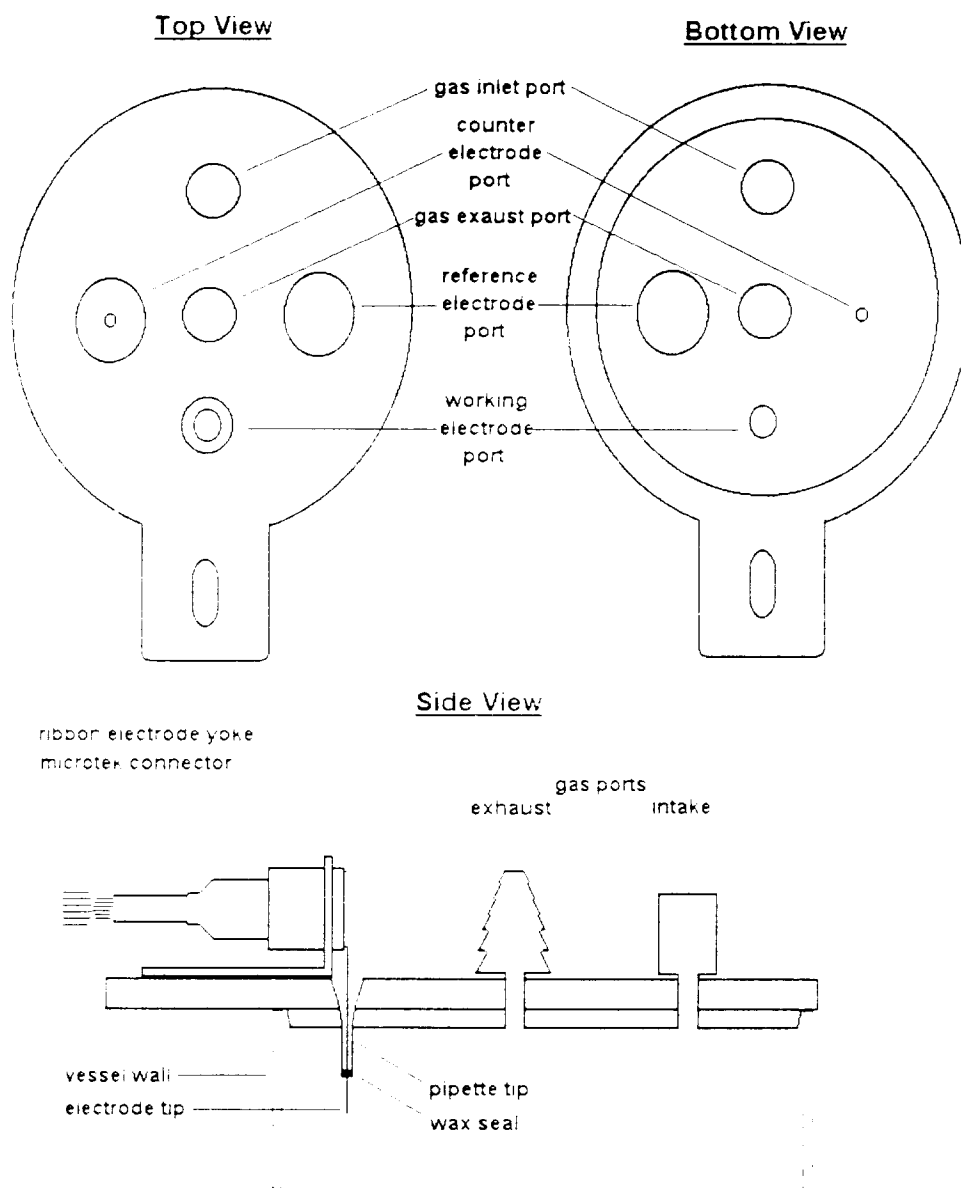


Figure 2.2 Schematic diagram of lid for test cell used for electrochemical measurements of the U. Michigan ribbon-cable probes.

the ribbon cable is mounted on the lid and provides a firm anchor for the leads to the electronic instrumentation. The reference electrode is a double junction Ag/AgCl electrode, No. MI-403, from Microelectrodes, Inc., Londonderry, New Hampshire. The counter electrode is a 0.05 cm diameter Pt wire mounted in Kel-F, No. MW1032, from Bioanalytical Systems Inc., West Lafayette, Indiana. The Pt wire extends about 3 to 4 cm into the electrolyte to give an area approximately 0.5 cm².

2.2. U. Michigan Ribbon-Cable Probe 1, Site 1.

Electrochemical studies on site 1 of U. Michigan ribbon-cable probe 1 were continued this quarter. Test procedures and results of the first 35 days of electrochemical testing were described in the Quarterly Progress Report No. 5. This quarter an abbreviated cyclic voltammetry test protocol was employed to monitor the electrode status during the long term soaking period from 35 days to 108 days. Data was collected at scan rates of 0.05, 10, 20, 50, 100 and 200 V/s. The measurements were made by sweeping the potential from +0.1 V to -0.4 V, then to +0.2 V and back to +0.12 V vs. Ag/AgCl in a solution of deaerated 0.1M PBS solution. The current in the negative going sweep at 0 volts vs. Ag/AgCl was taken as the residual current and used to calculate the apparent capacitance from which the electrochemical surface area is estimated as discussed below. Fresh PBS solution was put in the cell prior to each scan rate study and deaerated for 1-2 hours before beginning the study. The probe was soaked in PBS solution between scan rate studies.

Table 2.1 lists the background current obtained from the seven studies performed this quarter along with the comparable data from the complete scan studies conducted last quarter. Figure 2.3 plots the apparent capacitance, C_{app} , as a function of the scan rate for each study. C_{app} is calculated by dividing the current at 0 V vs. Ag/AgCl by the scan rate, thus $C_{app} = Q/V = I/v$, where v is the scan rate. Theoretically, C_{app} will approach a constant value at high scan rates where there are no contributions to the current from faradaic reactions. The apparent capacitance is essentially a d.c. measurement of the double layer capacitance. There will be no contribution from other sources of capacitance such as the ribbon leads. This capacitance, therefore, is not equivalent to that determined by the impedance measurements at 1 kHz.

Table 2.1 Current measurements for the ten scan rate studies on site 1 of U. Michigan ribbon-cable probe No. 1.

Study No.	Days Soaked	v (V/s)	0.05	10	20	50	100	200
Current (nA) ^a								
1	0		0.096	6.2	11.0	26.8	45.5	79.5
2	8		0.138	9.9	18.8	11.6	15	126
3	35		0.142	11.8	21.4	45.0	79	134
4	52		0.150	12.4	21.8	48.5	83.5	138
5	59		0.144	12.3	21.4	46.0	78.5	130
6	70		0.148	12.2	21.4	46.0	82.0	129
7	76		0.156	11.8	21.2	46.0	82.5	127
8	91		0.240	22.0	42.5	109.5	151	264
9	100		0.226	33.0	58.0	128	230	365
10	108		0.334	34.5	63.0	136	246	400

^a Current at 0.0 V vs. Ag/AgCl 3 M NaCl measured from voltammogram taken in PBS.

The electrochemical surface area (ESA) of the electrode is determined by dividing the apparent capacitance by the specific double layer capacitance of iridium metal. It is difficult, however, to know what value to use since it will depend on the real surface area of the metal as well as the electrolyte. We have measured the apparent capacitance on a large area Ir wire electrode in PBS at 0.0 V vs. Ag/AgCl and determined that the specific capacitance is 65 $\mu\text{F}/\text{cm}^2$ geometric [1]. Mazota and Conway reported that a comparison of the real and geometric areas based on H atom desorption measurements showed that typical roughness factors for polished iridium was 2.5 to 3 [2]. Correcting the value of 65 $\mu\text{F}/\text{cm}^2$ for roughness would give a value of 22 to 26 $\mu\text{F}/\text{cm}^2$ real. These values are close to the value of 32 $\mu\text{F}/\text{cm}^2$ real reported for Ir metal in presence of chloride comparable to that in PBS [3]. We will continue to use the value of 25 $\mu\text{F}/\text{cm}^2$ to calculate the electrochemical surface area based on capacitance. Despite this uncertainty in the absolute magnitude of the ESA based on capacitance, changes in the value for one electrode and comparisons between electrodes with the same type and geometry of Ir provide a useful method to monitor differences in the condition of the electrodes.

The ESA calculated from the C_{app} values at 200 V/s for the ten studies are listed in Table 2.2. The ESA increased from 1590 μm^2 to 2520 μm^2 in the 8 days between studies 1 and 2. The electrochemical area estimates from the steady state current in the Ru study, discussed last quarter, was essentially unchanged during this period. During the next 68 days, the ESA

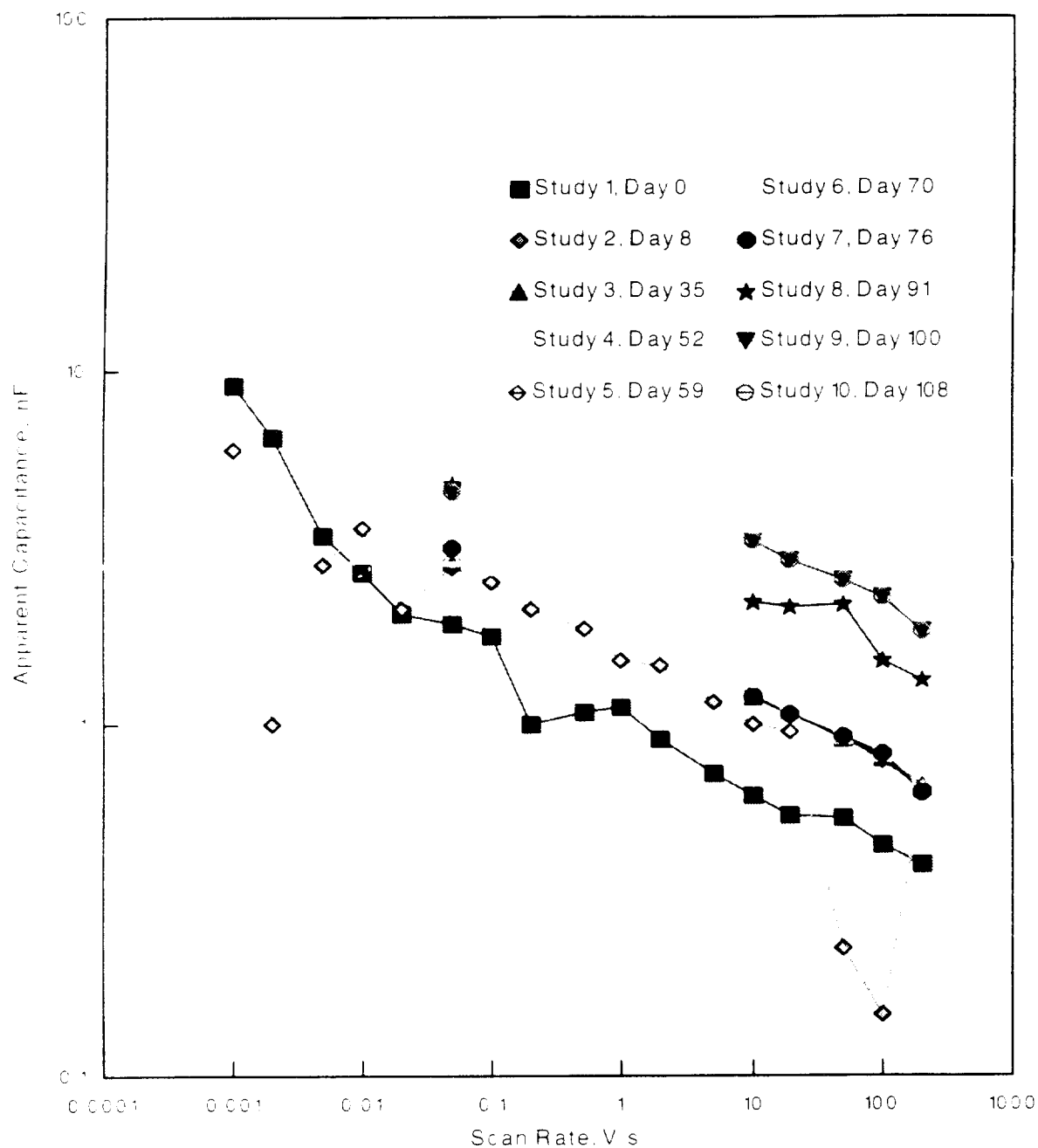


Figure 2.3 Comparison of apparent capacitance of site 1 on U. Michigan ribbon-cable probe No. 1 calculated from the currents in Table 2.1 for the ten scan rate studies.

Table 2.2 Dimensions of site 1 on U. Michigan Ribbon Cable-Probe No. 1.^a

Study No.	Days Soaking	Area from C_{app} (μm^2) ^b
1	1-2	1590
2	7-8	2520
3	35	2680
4	52	2760
5	59	2600
6	70	2580
7	76	2540
8	91	5280
9	100	7300
10	108	8000

^a Nominal area of electrode site is $600 \mu\text{m}^2$.

^b Calculated from current measured at 200 V/s in PBS using double layer capacitance of Ir metal of $25 \mu\text{C}/\text{cm}^2$.

fluctuated slightly with its highest value reaching $2760 \mu\text{m}^2$, returning to $2540 \mu\text{m}^2$ on day 76. Between the 76th and 91st day, however, there was a significant increase in the ESA to $5280 \mu\text{m}^2$. From here the ESA continued to increase with each scan rate study, finally attaining a value of $8000 \mu\text{m}^2$ by the 108th day of soaking.

As discussed in Quarterly Report No. 5, the observed increase in the residual current could be caused by one or a combination of three factors: insulation failure, formation of oxide, and/or reduction of oxygen. The overall shape of the cyclic voltammograms did not change significantly over the soaking period indicating little deterioration of the insulation. Figure 2.4 shows the cyclic voltammograms measured at 0.05 V/s and 200 V/s for day 35 and day 108. The cathodic peak at -0.1 V vs. Ag/AgCl evident at the 0.05 V/s scan rate could be due to reduction of either iridium oxide or oxygen in solution or adsorbed on the electrode.

To evaluate the cause of the increased residual current, the potential window for the cyclic voltammogram was extended to +0.6 V vs. Ag/AgCl to include the region where the oxidation-reduction reactions of iridium oxide occur. Figure 2.5 shows two cyclic voltammograms on site 1 over the extended potential window, the first taken on day 34 and the second on day 113. The peaks centered around +0.2 V vs. Ag/AgCl indicate the presence of some oxide on the electrode even though it was never intentionally activated. The current in these peaks is larger in the CV taken after 113 days of soaking indicating additional oxide on the

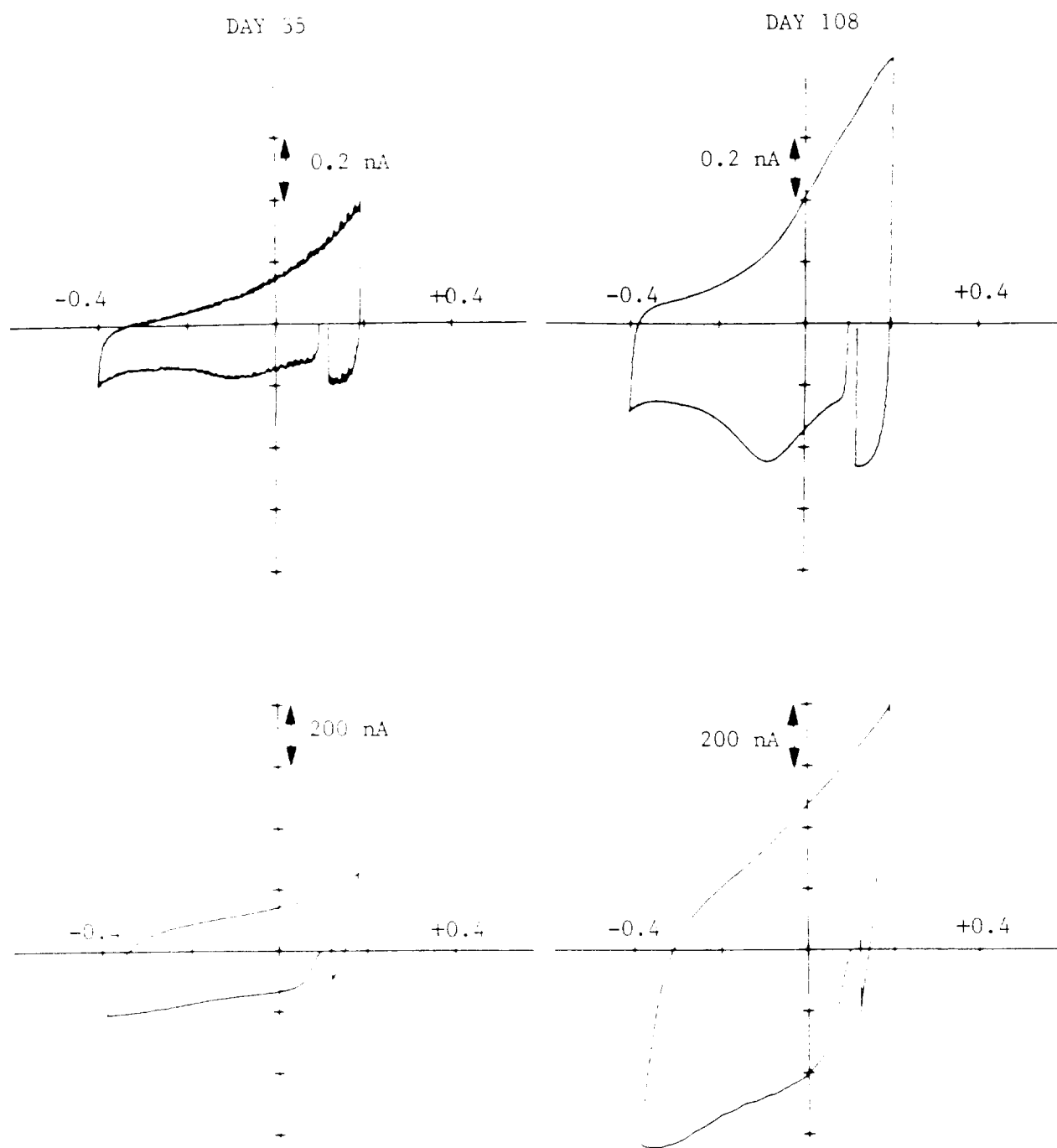


Figure 2.4 Comparison of the cyclic voltammograms of site 1 on U. Michigan ribbon cable-probe no. 1 acquired on day 35 (left) and day 108 (right). The apparent capacitance was determined from the current at 0 V in the 200 V/s scan rate. The electrolyte was deaerated 0.1M PBS and the potential scale is referenced to Ag/AgCl.

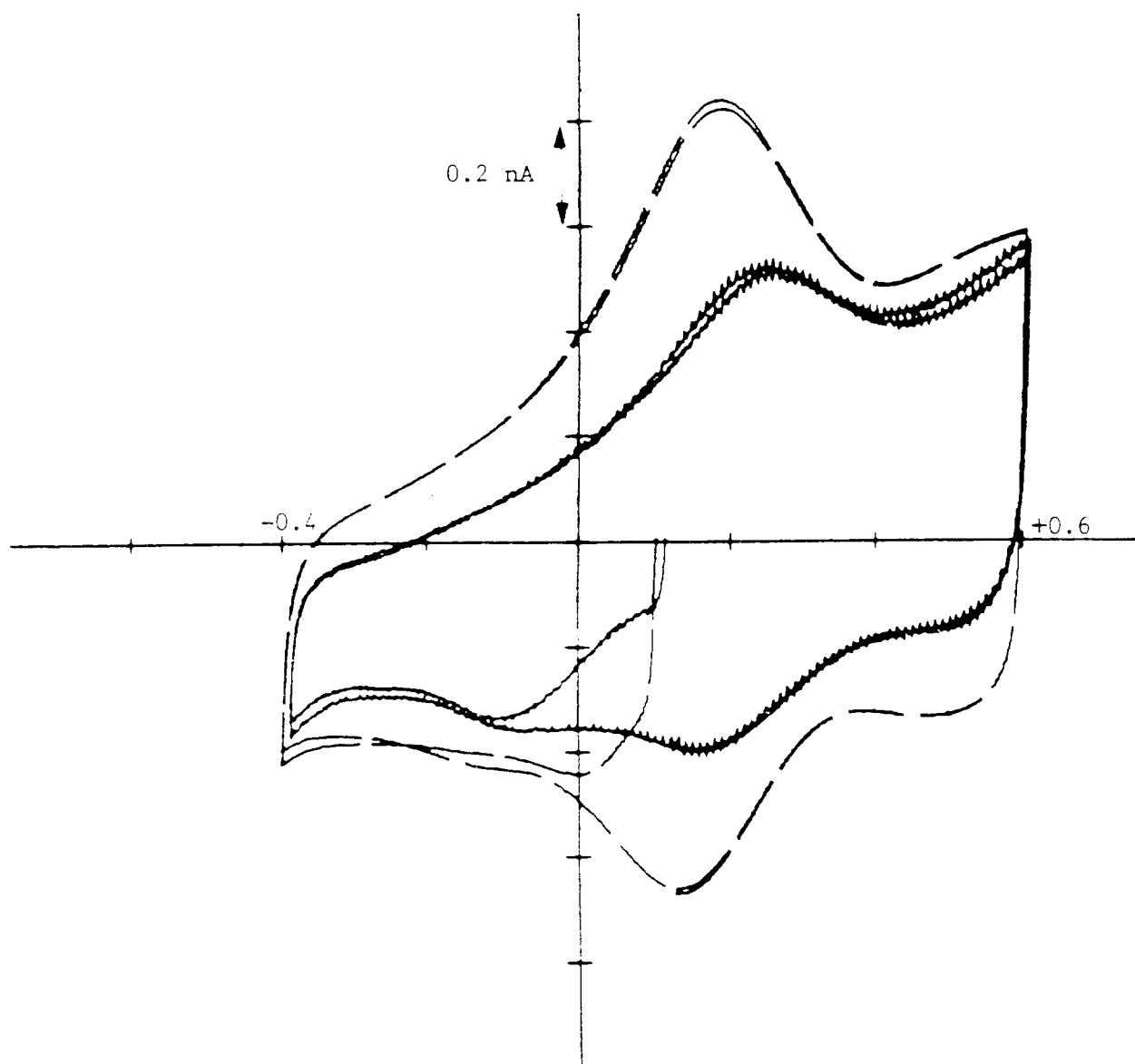


Figure 2.5 Comparison of voltammograms over a wide potential range to evaluate oxide growth on U. Michigan ribbon cable-probe no. 1 site 1 acquired on day 34 (solid line) and day 113 (broken line). Electrolyte: deaerated 0.1M PBS. Scan Rate: 0.05V/s. Potential scale: V vs. Ag/AgCl.

electrode. We believe the cathodic peak at -0.1V vs. Ag/AgCl seen at 0.05 V/s in Figure 2.4 is the reduction of oxide. The lower positive limit of the cyclic voltammogram shifts the oxide peak to more negative potentials than in Figure 2.5. The additional oxide found after longer soaking times may explain the increase of the current in the scan rate studies given in Table 2.1. If this is the case, then the areas calculated from the current measured at 200 V/s are not correct because the capacitance per unit area for iridium oxide is larger than the value of $25 \mu\text{F}/\text{cm}^2$ used for bare Ir metal. For these measurements, therefore, it is not necessary to invoke the presence of residual oxygen in the electrolyte to explain the apparent increase in the geometric area of the electrode.

2.3. U. Michigan Ribbon-Cable Probe 2, Site 5.

Another ribbon-cable probe with Ir microelectrodes from the U. Michigan group was tested to demonstrate if the presence of oxygen in the system is leading to activation of the electrode during the area determination using the Ru technique. The U. Michigan did not measure the impedance at 1 kHz of this electrode before sending it to us to assure that there was no "preactivation." Prior to placing the probe into Ru hexaammine solution for the scan rate study, the probe was placed in PBS solution that had not been deaerated. This solution will be referred to as "non-deaerated" PBS. The electrode was then cycled at 0.05 V/s from an initial potential of +0.05V vs. Ag/AgCl to -0.4V, up to +0.5V, back to -0.4V and then returned to +0.05V. This voltage sequence insured that any oxide present would be in its reduced state. Moreover, the potential window also should detect the presence of any oxide on the Ir metal. The current in the cyclic voltammograms of sites 1, 3 and 4 of the probe was unusually small, although there was continuity. The CV's for sites 2, 5 and 6, shown in Figure 2.6, had currents comparable to that of the previously tested ribbon electrodes and showed no evidence of being "activated." Site 5 was chosen for further testing because it is farthest from the solution-atmosphere interface (see Figure 2.1).

Cyclic voltammograms were measured over the sweep rates from 0.001 to 200 V/s in solutions with Ru hexaammine dissolved in phosphate-buffered saline, pH 7.3 (PBS). After the Ru hexaammine portion of the study, a CV in non-deaerated PBS was taken. Comparison of the cyclic voltammograms in non-deaerated PBS at 0.05 V/s of site 5 before and after the Ru

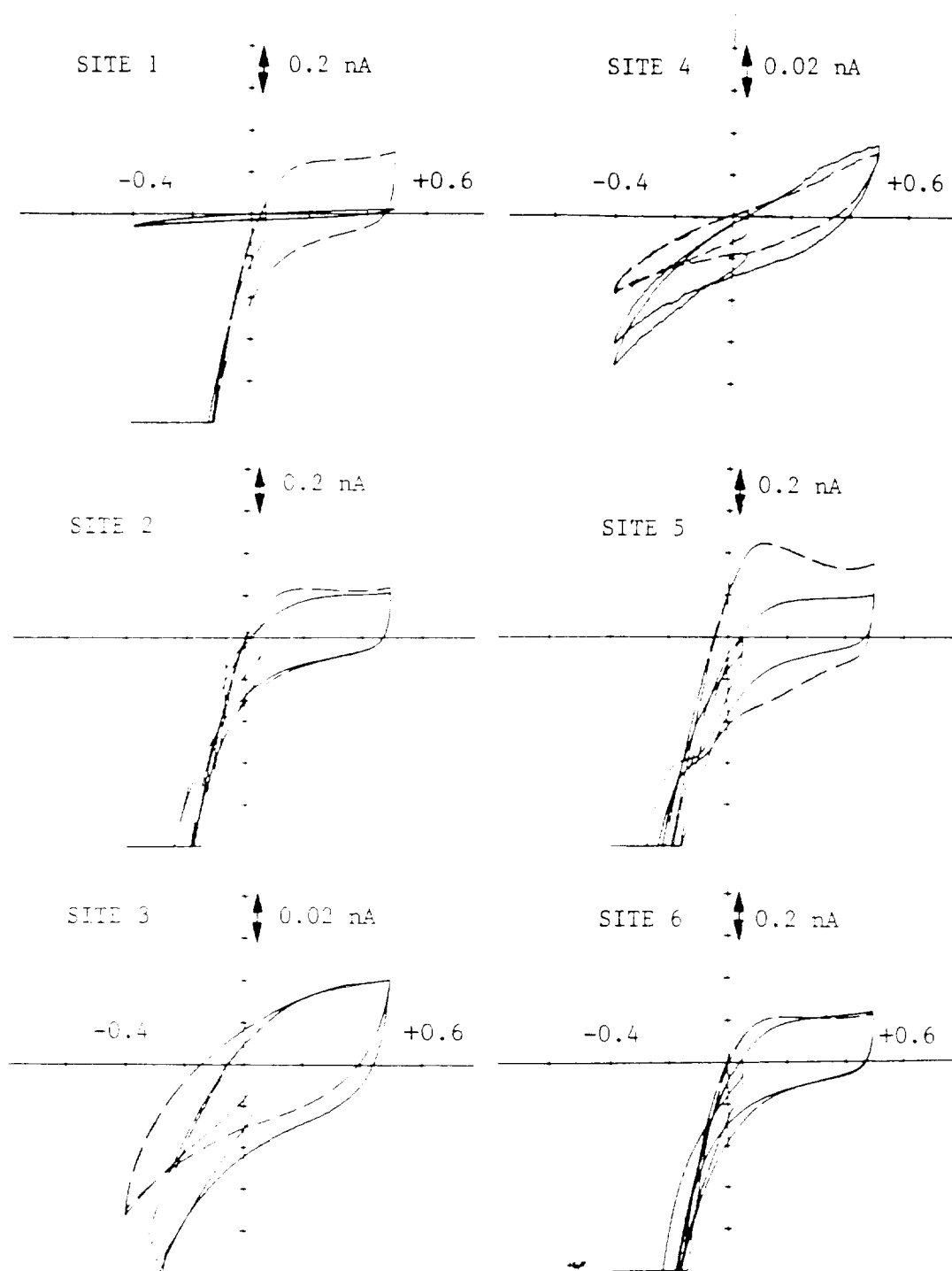


Figure 2.6 Cyclic voltammograms of the six sites on the U. Michigan ribbon-cable probe No. 2 in non-deaerated 0.1 M PBS at 0.05 V/s before and after the scan rate study on site 5. Potential scale: V vs. Ag/AgCl.

hexaammine measurements shown in Figure 2.7 reveal that the site was somewhat activated during the study. Background measurements at each scan rate were then taken in deaerated PBS.

After the background measurements in PBS, each site was cycled again using the wide potential window in 0.1 M PBS that was aerated. The CV's are shown in Figure 2.6 to compare with those obtained before the Ru scan rate study. The CV on site 5, the tested electrode, indicate significant oxide growth while those on sites 2 and 6 show evidence of slight activation. For sites 3 and 4, the CV's show little activity as was observed before the ruthenium hexaammine testing. The most dramatic change was in the CV for site 1. After the scan rate study, the CV was more similar to those on sites 2 and 6, whereas before the study it resembled the CV's on site 3 and 4. This site may have been "dirty" with some insulating contamination and became clean during the soaking period in solution.

The voltammetric data from the scan rate study corrected for the charging and residual current are listed in Table 2.3. No results are listed for sweep rates above 0.1 V/s because the currents in the background voltammogram at potentials before the Ru reduction wave were larger than those obtained when the ruthenium hexaammine depolarizer was present. Because of these large background currents we also could not observe the distinct cathodic and anodic peaks expected at higher scan rates. The enhanced background can be caused by incomplete removal of oxygen in the background PBS, the presence of oxide on the iridium, or some aspect of the structure of the electrode itself, such as an edge effect or porosity of the Ir film. Oxygen can be excluded because at the slower scan rates there was no significant current observed for oxygen reduction. As mentioned above, however, site 5 did appear to have some oxide on it.

The corrected voltammograms obtained at scan rates from 0.001 to 0.010 V/s were sigmoidally shaped and the forward and reverse peaks coincided. The maximum current was independent of scan rate, and is thus the steady state current, i_{ss} . From 0.020 V/s to 0.100 V/s the forward and reverse curves coincided at the plateau but were separated on the falling and rising portions of the voltammogram. Since there were no peaks observed in the voltammograms, we have used i_{ss} instead of i_p to designate the maximum current at the plateau. The half wave potentials, $E_{p/2}$, are constant indicating little iR drop, but lie negative of the value of -0.170V vs. Ag/AgCl which is obtained on Ir metal under conditions of linear diffusion control. The absolute values of the current function, $(i/v)^{1/2}$, decrease with increasing scan rate throughout the range of scan rates.

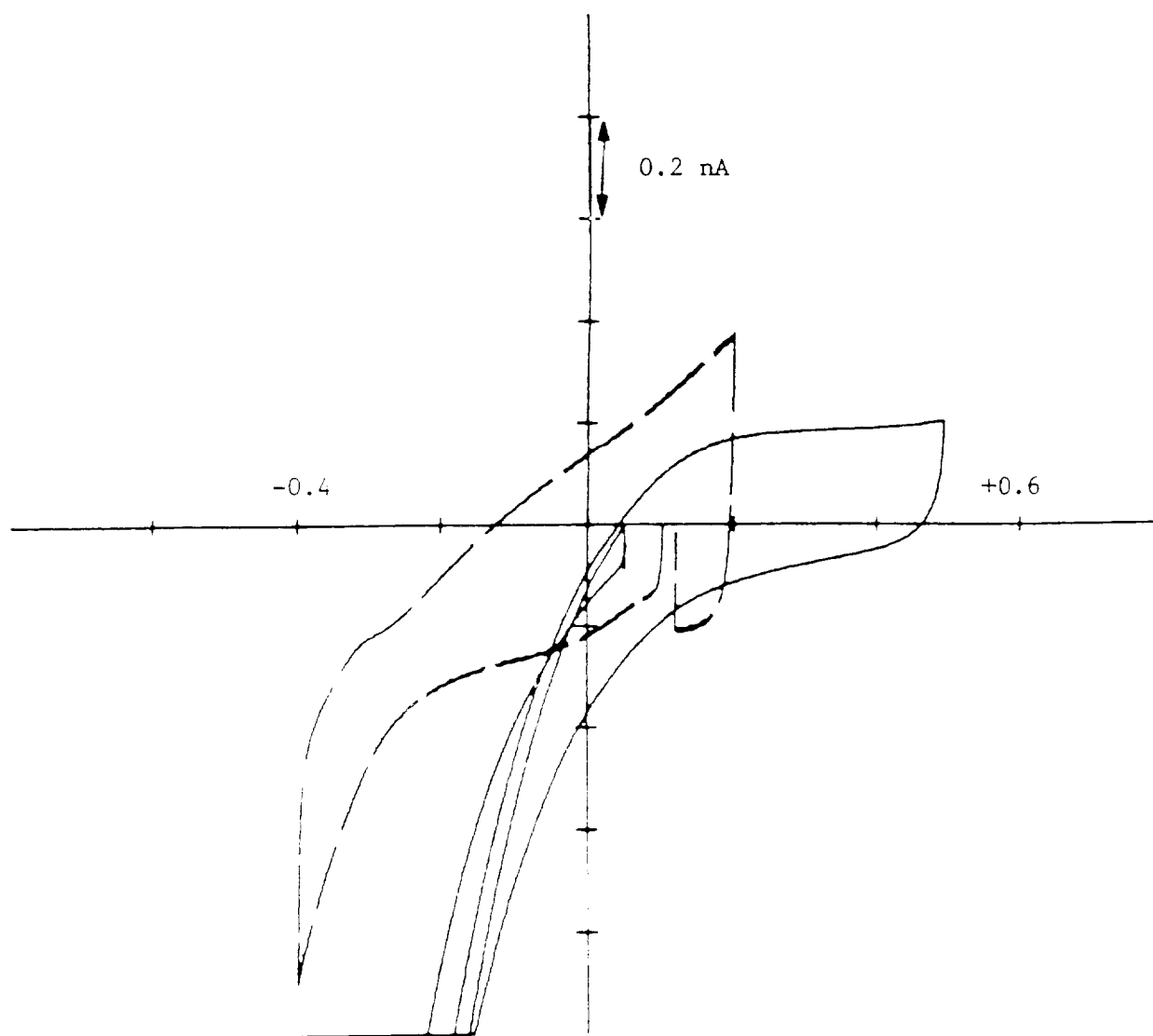


Figure 2.7 Cyclic voltammograms of site 5 of U. Michigan ribbon-Cable probe No. 2 before (solid line) and after (broken line) Ru hexaammine portion of the scan rate study. Scan rate: 0.05V/s. Electrolyte: non-deaerated 0.1M PBS. Potential is given as V vs. Ag/AgCl

Table 2.3 Data for electrochemical study 1 on site 5 of U. Michigan ribbon-cable probe No. 2^a

Scan Rate (V/s)	Half-Wave Potential ^b E _{1/2} (V)	Maximum Current i _m (nA)	Current Function i _m v ^{-1/2} (nAV ^{-1/2} s ^{1/2})	Disk Radius ^b (μm)
0.001	-0.19	-4.66	-147	13.6
0.002	-0.19	-4.68	-105	13.5
0.005	-0.19	-4.60	-65.1	13.1
0.010	-0.19	-4.66	-46.7	13.1
0.020	-0.19	-4.74	-33.5	13.1
0.050	-0.19	-4.94	-22.1	13.0
0.100	-0.19	-5.14	-16.3	12.8

^a Reduction of ruthenium hexaammine in a solution of 1.34 mM Ru(NH₃)₆Cl₃ in PBS corrected for residual and charging current in PBS alone. Potentials are vs. Ag/AgCl/3 M NaCl.

^b Calculated from the maximum current using Eqs. (1) and (2) which assume electrode is a disk.

These results are consistent with the site behaving like a disk electrode under conditions in which the mass transport is controlled by nonlinear diffusion.

The data were fit to the equation we used previously to calculate the radius of the electrode, r , assuming it has the same area as a disk [4,5].

$$i_p = 4C_0 \exp(-\alpha FRTD_0^{-1/2})^{1/2} = 0.34p \exp(-0.66p) + 0.66p - 0.13p \exp(-11/p) + 0.35p^2 \quad (1)$$

Where C_0 is the concentration of the ruthenium hexaammine in mol cm⁻³, F is Faraday's constant, R the gas constant, T the absolute temperature, D_0 the diffusion coefficient for the ruthenium hexaammine in PBS, 6.54×10^{-6} cm² s⁻¹, and p is

$$p = E_0 \frac{nFv}{D_0 RT} \quad (2)$$

The results are given in the last column of Table 2.3. There is a steady decrease in the radius, as the sweep rate increases. For the two slowest scan rates, the corresponding area of the electrode is 680 μm² which agrees very well with the geometric area.

Using an average value of 4.65 nA for the steady state current in the equation for the current at a disk electrode, Eq. (3), a value of 13.4 μm is obtained for the radius of the electrode.

$$r = i_{ss} / 4nFCD \quad (3)$$

This value is very close to those of 13.5 μm and 13.2 μm obtained from the first two scan rate studies on site 1 of ribbon cable probe No. 1 reported in Quarterly Report No. 5. The value is not significantly different than that derived from Eqs. (1) and (2).

A constant value for the current function at the higher scan rates indicative of linear diffusion was not obtained within the limited range of scan rates for which background-corrected voltammograms were available. However, the plot of $i_m v^{-1/2}$ vs. $v^{-1/2}$ was linear over the range of scan rates 0.001 to 0.1 V/s, characteristic of non-linear diffusion. Using the relationship between the maximum current and the scan rate developed by Nicholson and Shain [6] for a spherical electrode, Eq. (4), we calculated the radius and area, A, of the site from the intercept and slope, respectively.

$$i_m / v^{1/2} = (0.724 \times 10^{-5}) \frac{nCD A}{r} \frac{1}{v^{1/2}} + (2.69 \times 10^{-5} \text{ m}^3 \text{ s}^{-1/2} CD^{1/2} A \quad (4)$$

The values obtained from the fit to Eq. (3) were 1.45 μm for the radius and 103 μm^2 for the area. These values are very different from those based on the steady state currents at low scan rates. In addition, there is no agreement between the value of the area calculated from the radius and that determined directly from the fit of the data. The inconsistency of the results is due to the sensitivity to the value for the intercept. For our data, which is taken over such a short range of slow sweep rates, the intercept is poorly defined despite the good linearity of the plot of $i_m v^{-1/2}$ vs. $v^{-1/2}$. The radius values calculated from Eqs. (1) -(3) are considered more reliable.

The values of the steady state radius and area are virtually identical to those values calculated for site 1 on ribbon-cable probe No. 1 from the first scan rate study. This observation indicates the electrochemical behavior of the two sites, R1-S1 and R2-S5, was similar in the slow sweep rate region of the scan rate study. However, the electrochemical surface area calculated from the apparent capacitance at 200 V/s of 4560 μm^2 for R2-S5 was almost 3 times that for site 1 on ribbon cable No. 1. The area of site 1 did not reach a comparable value until the probe had been soaked for 91 days when area based on the capacitance at 200 V/s reached 5280 μm^2 . The

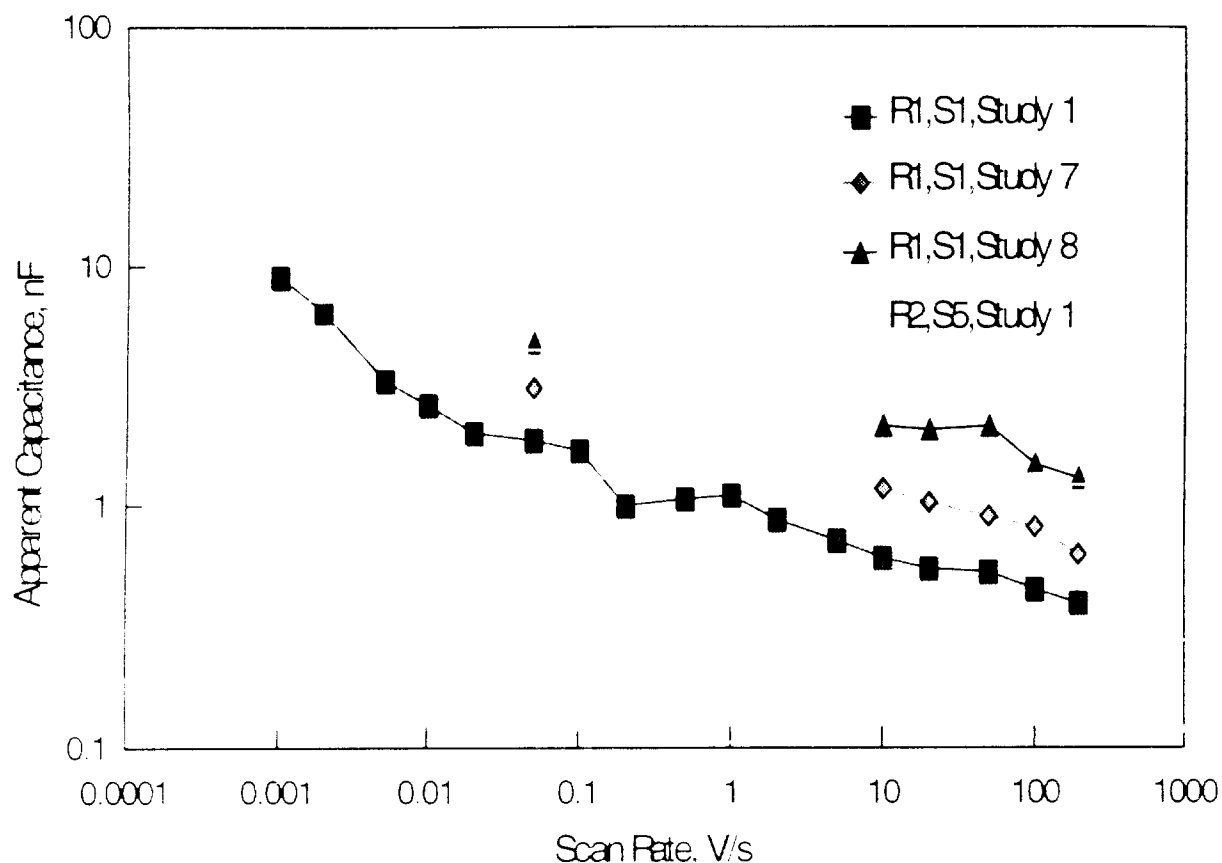


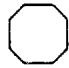







Figure 2.8 Comparison of C_{app} determined in three scan rate studies for Ribbon Cable-Probe 1 site 1 and one study of Ribbon Cable-Probe 2 site 5.

C_{app} for the two electrode sites are plotted in Figure 2.8. The higher values of C_{app} could be attributed to the activation of the Ir sites or to the structure of the electrode discussed below.

Table 2.4 summarizes the electrochemical measurements that have been made on U. Michigan sputtered iridium planar electrodes by EIC Laboratories in this contract and previous years [4,7]. Also included are the results for an Ir wire ultramicroelectrode with a faceted surface obtained from the Huntington Medical Research Institute. The ribbon cable electrodes have the smallest geometric areas of the U. Michigan samples evaluated. The steady state currents from the three studies are very similar and give an ESA at the slow scan rates that is close to the

Table 2.4 Comparison of electrochemical testing of U³⁺ Michigan sputtered film and HMRI wire microelectrodes.

Electrode	Shape	Nom A (μm^2)	Ru Conc (mM)	i_p (nA)	SS ^a	radius disk (μm) Aoki ^b	SS	E _{SA} (μm^2) Cap ^c	Comments
SX-01 #23 site 5		1000	3.3	16	19	17.7	1130	6500	data to 5 V/s peaks ≥ 0.05 V/s
SX-01 #23 site 3-		1000	3.3	13	15.7	14.8	774	1000	data to 5 V/s no peaks to 200 V/s
CN8 #49 site 1, study 1		800	1.18	4.0	13	13.3	547	1710	data to 200 V/s peaks ≥ 0.5 V/s
CN8 #49 site 1, study 2		800	1.20	19	62	---	12080	5780	data to 50 V/s peaks ≥ 0.2 V/s
Ribbon-cable #1 site 1, study 1		600	1.38	4.8	13.5	13.3	572	1590	data to 0.5 V/s no peaks to 0.5 V/s
Ribbon-cable #1 site 1, study 2		600	1.32	4.5	13.2	---	547	2520	data to 1.0 V/s no peaks to 1.0 V/s
Ribbon-cable #2 site 5, study 1		600	1.34	4.7	13.4	13.5	565	4560	data to 0.1 V/s no peaks to 0.1 V/s
HMRI-IC-06-02		480	3.3	11.6	13.6	13.1	580	3000	data to 100 V/s peaks ≥ 0.5 V/s

^a Radius and area calculated from steady state current at the lowest scan rate using Eq. (3) assuming disk geometry.

^b Calculated from current function at low scan rates using Eqs. (1) and (2).

^c Area determined from apparent capacitance based on background current at high scan rate and $25 \mu\text{F}/\text{cm}^2$ for iridium.

geometric area. This area and the shape of the cyclic voltammograms has remained relatively stable for much longer periods with the ribbon cable probes than for previous electrodes in which the electrolyte penetrated contacts on the pc boards. The ESA based on the high sweep rate capacitance measurements, however, are significantly larger than the geometric areas and are more variable from electrode site to electrode site. In addition, the data from the Ru scan rate studies were limited to scan rates of ≤ 0.5 V/s because of the problem with the background correction. Data from the somewhat larger U. Michigan electrodes could be used at rates above 5 V/s. It is possible that the difference between the two electrochemical responses is related to the new modified site formation techniques now being used by U. Michigan [8] to eliminate previous problems with adhesion of the Ti/Ir to the polysilicon interconnects. The electrode site is etched in a buffered HF which leads to some undercutting of the dielectric layers on the polysilicon conductors. If the subsequently sputtered metal film does not make a good seal between the polysilicon and the dielectric (see Figure 5 in Ref. 8), the electrode will have a poorly defined geometry at its edge. The structure could result in increased porosity of the film, trapping of oxygen in the voids, and/or a thin layer of electrolyte between the oxide and metal leading to nonuniform current distribution. Any of these conditions may lead to the background problems we have observed at the higher scan rates.

3. ELECTROCHEMICAL IMPEDANCE SPECTROSCOPY

Last quarter we measured the electrochemical impedance spectroscopy (EIS) on site 1 of ribbon-cable probe No. 1 as part of the characterization studies. The impedance was reported for measurements at 1 kHz for different bias potentials on the electrode. There was an increase in the impedance at more negative potentials as expected since the voltammograms showed oxide was present and the resistance of the oxide increases as it is reduced. There is potentially a great deal more information available from EIS than that obtained from the single impedance value taken at 1 kHz. In Quarterly Report No. 3, data from impedance measurements over a range of frequencies was presented on a U. Michigan CN8-49 probe which had five sites with geometric area of $800\text{ }\mu\text{m}^2$. Interpretation of this data was hindered by leakage at the sites and shorting between the sites after long term soaking. The impedance measurements on each site were also limited to a single bias potential. This quarter we made complete EIS measurements on a site on a new ribbon cable that had not been subjected to previous testing and began the analysis of the data. The goal was to understand the impedance of bare Ir before proceeding to the activated Ir site.

3.1. Experimental Protocol for EIS Measurements

Ribbon-cable probe No. 4 was mounted in the new electrochemical cell and a cyclic voltammogram on site 2 was measured in deaerated PBS over the potential range between +0.2 and -0.4 V vs. Ag/AgCl. The CV, however, showed that there was still some oxygen present. After several hours of degassing, there was still evidence of oxygen. The degassing was stopped, and the air above the cell was allowed to equilibrate with ambient air creating a condition between a deaerated and a non-deaerated solution. The EIS was run under this condition.

The EIS was measured using an M378-1 setup from EG&G. An a.c. signal was impressed on the bias voltage supplied by a PAR 273 potentiostat. The protocol for the EIS was to measure the impedance at each of a series of bias potentials over a frequency range of 10^{-2} to 10^4 Hz in three stages, 10^2 to 10 Hz, 10 to 10^{-1} Hz, and 10^{-1} to 10^{-2} Hz. The method used in the first stage was single 10 mV a.c. sine wave for the perturbation, while the latter two stages used a multiple sine wave with a 15 mV a.c. perturbation signal followed by a Fourier transform. The

initial measurement was made at -0.3 V vs. Ag/AgCl. The potential was then increased by 0.1 V increments up to a final potential of 0.5 V vs. Ag/AgCl. This protocol is different from that used on site 1 of ribbon-cable probe 1 for which the bias potentials were taken in a random sequence over the potential range. The data were analyzed using the EQUIVCRT.PAS program written by G. Boucamp [9]

Because complete deaeration was not achieved prior to the first EIS measurement, a second measurement was made in a solution that was successfully deaerated by sealing the lid of the cell more tightly. The CV's are compared in Figure 3.1(a). The smaller current in the region from -0.2 to -0.4 V vs. Ag/AgCl for the "pre EIS #2" showed reduced presence of oxygen. The very slightly higher current positive of 0.0 V vs. Ag/AgCl, however, indicated there was a little oxide on the electrode that was not evident in the CV before the first EIS measurement. After the EIS was repeated, a CV was again taken. The level of oxygen was comparable to that at the beginning of the first EIS measurement, but there was no indication of additional activation due the second EIS measurement

Table 3.1 summarizes the properties of the electrodes analyzed with EIS. The table shows that the impedance measurements at 1 kHz and a bias of 0.1 V vs. Ag/AgCl are in qualitative agreement with the CV data regarding the extent of oxide on the sites. Both measurements showed that the site with the least amount of oxide was site 2 of ribbon-cable probe No. 4 before the first test. The next least "activated" site was the same site used for the second EIS test. The CV of site 1 of ribbon 1, shown in Figure 3.1(b), shows a peak at -1.0 V vs. Ag/AgCl indicative of the presence of oxide. This site had been subjected to a full scan rate study with Ru as well as soaking in PBS for two days and had the most oxide on it. This oxide layer appears to have increased after the EIS. The amount of oxygen in the electrolyte or adsorbed on the electrode surface was smallest for the second EIS run on site 2, followed by the initial EIS run on site 2, and finally the EIS run on R1-S1. Thus, the desired condition of measuring the EIS on a site with minimal oxide and no influence from oxygen was not achieved. Nevertheless, the data provide important information on the effects of oxygen and a small degree of activation on the EIS

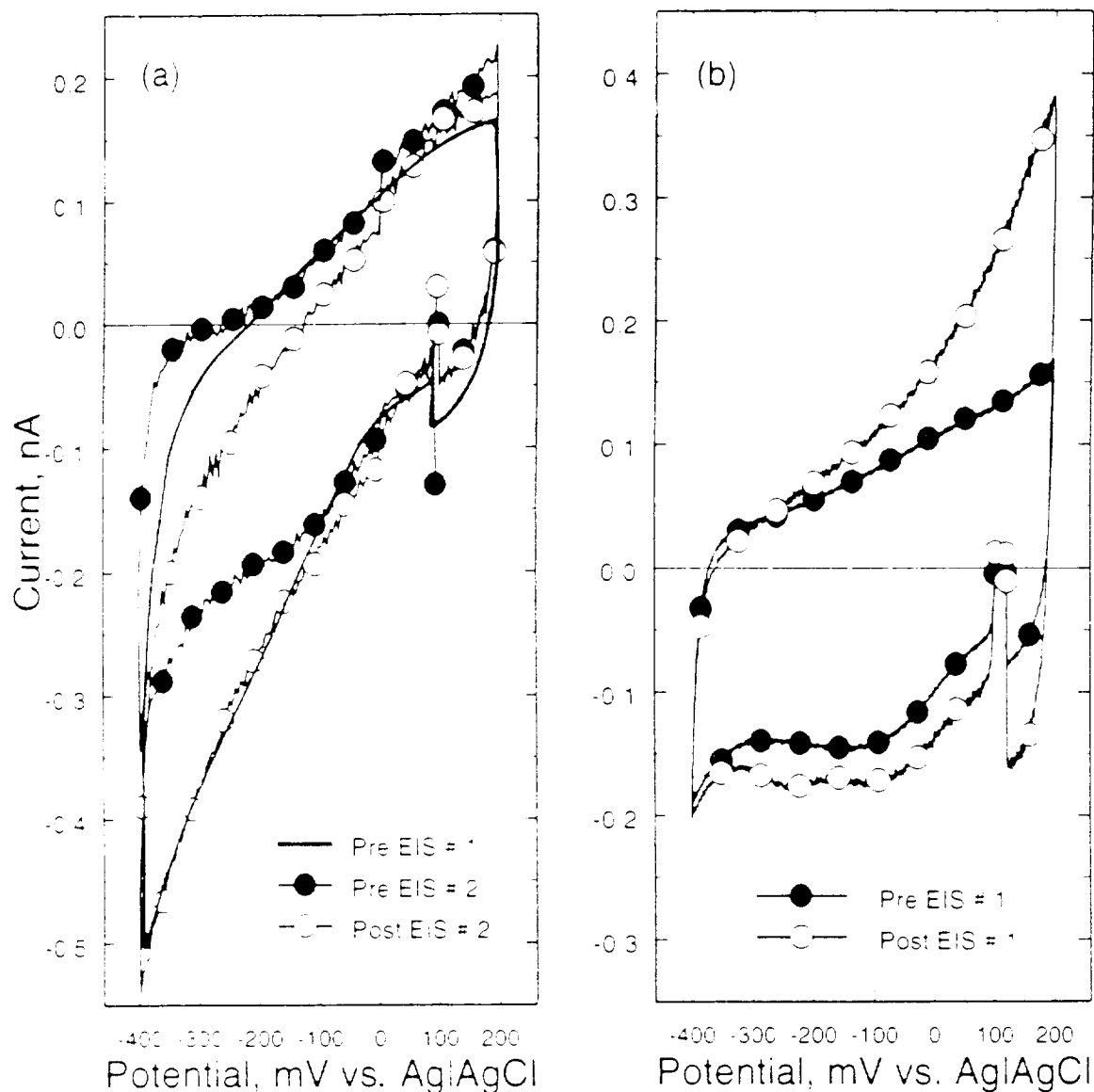


Figure 3.1 (a) Cyclic voltammograms of site 2 of U. Michigan ribbon-cable probe No. 4 before the first EIS measurement, and before and after the second EIS measurement. (b) Cyclic voltammograms of site 1 of U. Michigan ribbon-cable probe No. 1 before and after the EIS measurement. The electrolyte was 0.1 M PBS and the sweep rate was 0.05 V/s.

Table 3.1 Electrodes characterized with EIS

Electrode ^a	Impedance (k Ω m ²) ^b	PBS Electrolyte	Comments
R4-S2-I1	1600	partially deaerated	first exposure to PBS. CV shows no oxide evident initially
R4-S2-I2	780	deaerated	CV shows very thin oxide layer
R1-S1-I1	200	non-deaerated	previous Ru scan test. electrode soaked 2 days in PBS. CV shows thin oxide layer

^a R, S, and I refer to the ribbon number, the site number, and impedance measurement number, respectively.

^b Measured at 1 kHz in PBS on electrode biased at 0.1V vs. Ag/AgCl.

3.2. Three-Dimensional Plots of EIS Data

The data from the EIS are plotted in a three-dimensional Bode plot in Figures 3.2 to 3.4 for the three studies. The Bode plots explicitly show how the impedance magnitude, Z , and the phase angle, θ , vary with frequency. The phase angle is the angle between the current phase and that of the applied potential. A value of θ of 0° indicates the system is behaving like a resistor while a value of +90° means the system is reacting to the a.c. signal like a capacitor. These plots help to visualize the qualitative differences for the three measurements. The figures are in the order of increasing amounts of OXYGEN in the electrolyte, but the middle figure is the site with least amount of OXIDE. The most striking result from the comparison of the phase angle plots is the small phase angle obtained at low frequencies and negative bias indicating the system is behaving more like a resistor. The effect is most pronounced for the measurements made in the two electrolytes with the most oxygen. The potential region coincides with the reduction of oxygen which may be either in solution or adsorbed on the surface of the electrode. This reduction reaction is highly irreversible and thus will have a slow rate constant for electron transfer. The slow rate constant means the effect of oxygen reduction will be observed at low frequencies in the EIS as seen in Figures 3.3 and 3.4.

The other qualitative feature evident in the phase angle plots is the shape of the surface over the frequency range from 1 to 10^4 Hz. For the electrode site with the least oxide, Figure 3.3, as the frequency increases, there is a small hump peaking at about 10 Hz. This behavior is

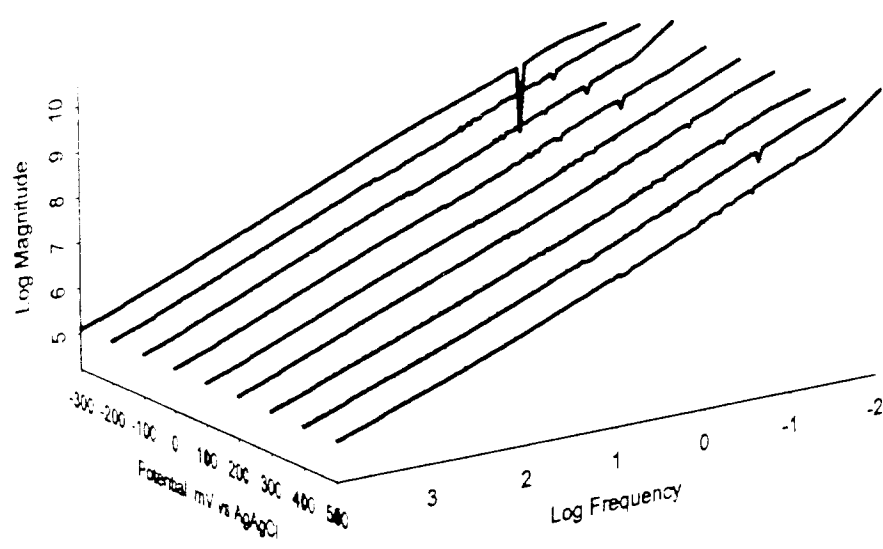
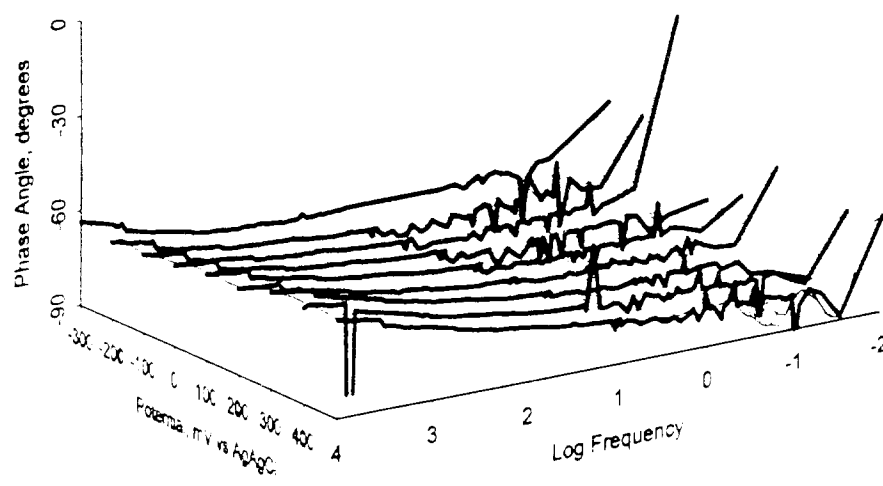


Figure 3.2 Three-dimensional Bode plots of EIS (study 2) of site-2 of U. Michigan ribbon-cable No. 4 taken in deaerated PBS.

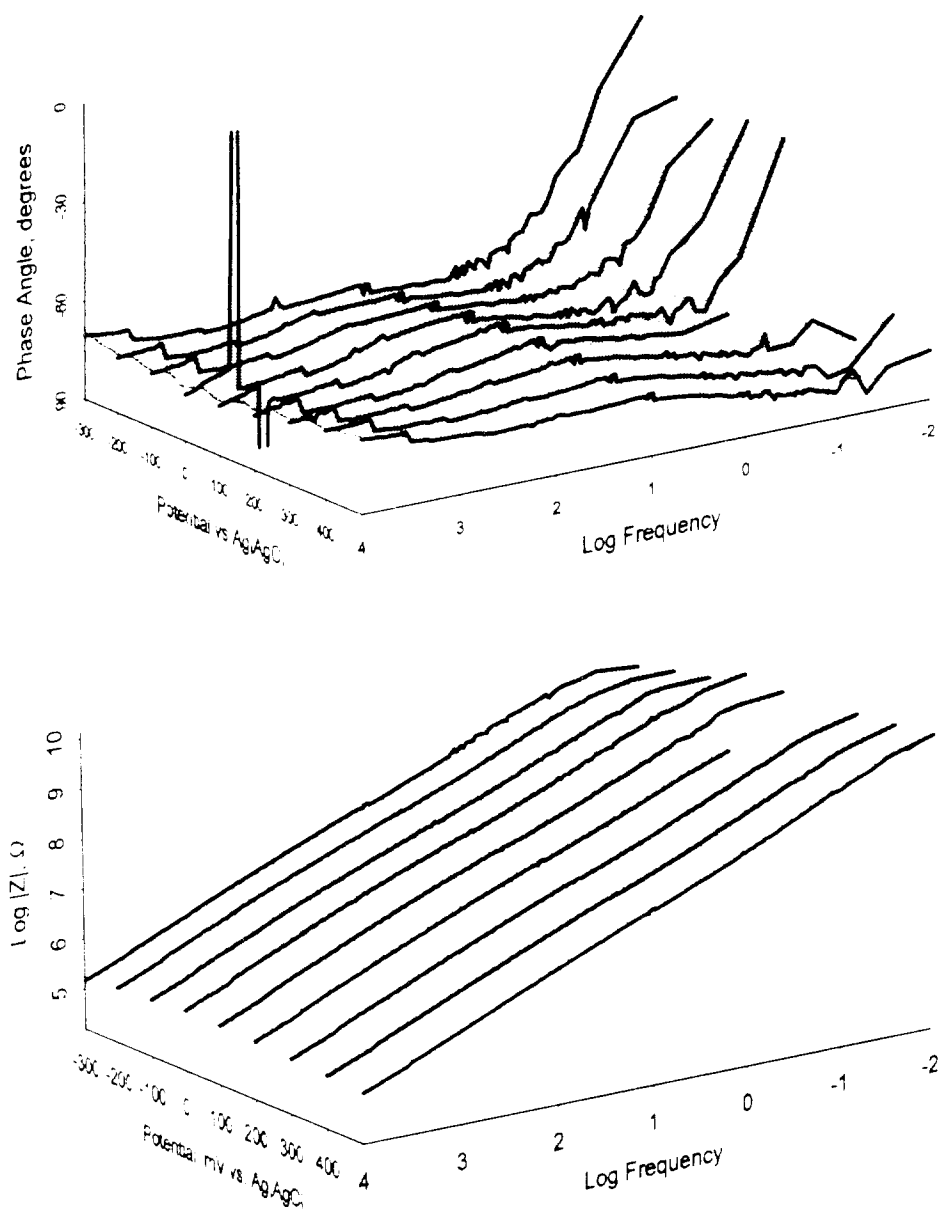


Figure 3.3 Three-dimensional Bode plots of EIS (study 1) of site-2 of U. Michigan ribbon-cable No. 4 taken in partially deaerated PBS.

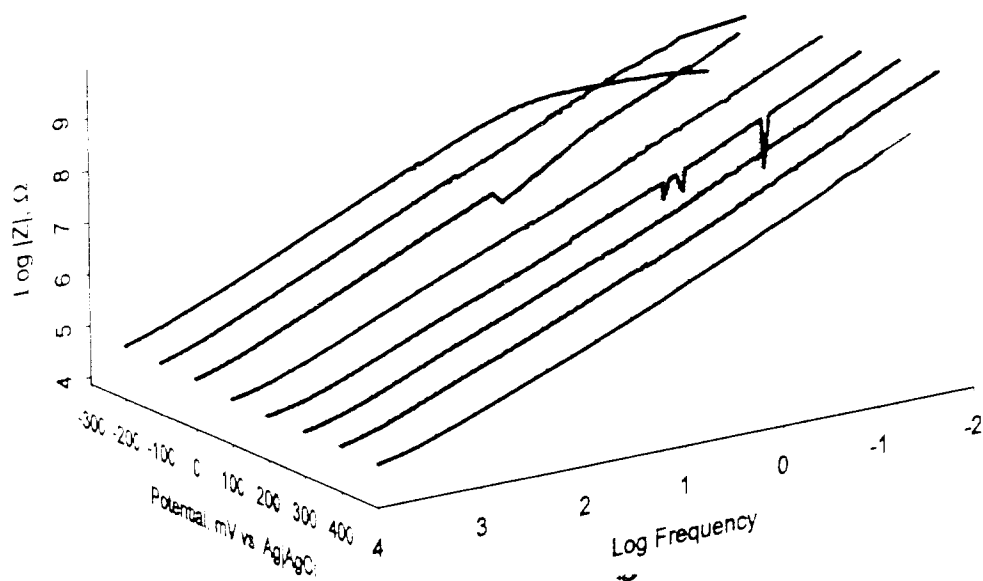
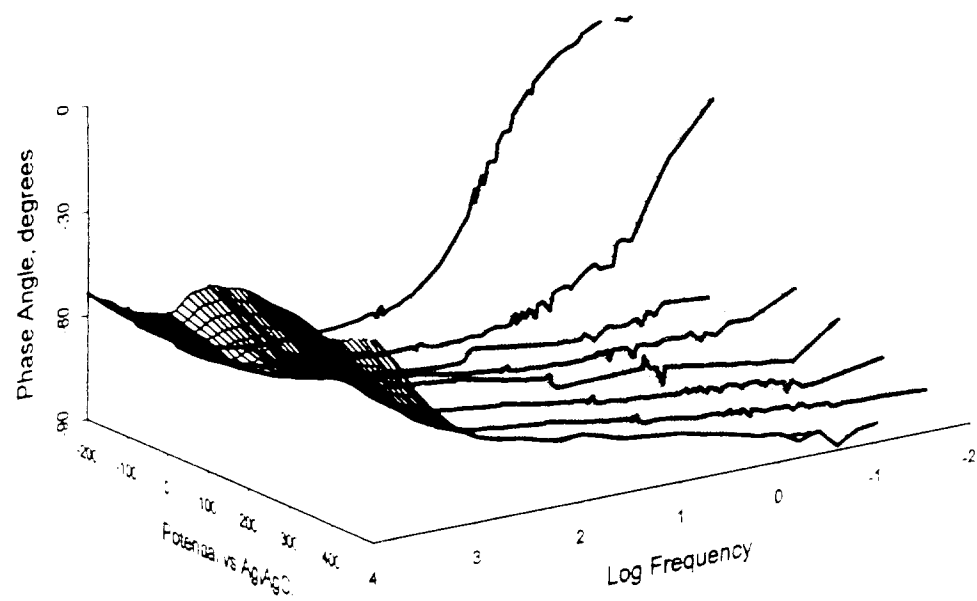


Figure 3.4 Three-dimensional Bode plots of EIS (study 1) of site-1 of U. Michigan ribbon-cable No. 1 taken in aerated PBS after completion of Ru scan rate study.

similar to that observed in the first impedance measurement on sites #3, 4, and 5 on probe CN8-49 (see Figure 2.4 of Quarterly Progress Report No. 3). For the site with a slight amount of oxide, Figure 3.2, the absolute value of θ decreases slowly with increasing frequency. Again, a comparable frequency dependence was observed on probe CN8-49 for the first impedance measurement on sites #1 and 2. For the site with the most oxide there is a steep decrease in the phase angle above 100 Hz. If the similar trends with frequency in the phase angle plots for the sites on CN8-49 reflect different amounts of oxide as we believe they do on the ribbon cables, the impedance measurements provide a sensitive method for detecting thin oxide layers. For the thin oxides layers, this dependence is relatively insensitive to the bias potential.

It is more difficult to see qualitative changes in the 3-D plots of the impedance values for the different electrodes. Figure 3.5 is a plot of the impedance at three frequencies vs. potential. The plot shows, as expected, that at all frequencies the impedance decreases as one proceeds from the electrode with the least oxide, R4-S2-I1, to that with the most oxide, R1-S1-I1. For both measurements on R4-S2 there is relatively little sensitivity to potential at frequencies above 10 Hz. This result reinforces the cyclic voltammogram data showing that the oxide layer is very thin on R4-S2-I2. There is the expected slight trend to higher impedance at negative potentials for R1-S1-I1 which is slightly more oxide. At the lower frequencies, there is a decrease in the impedance at negative bias when oxygen is present. The lower impedance, which corroborates the trend seen in the plots of the phase angle, reflects the low resistance path for electron transfer provided by the electrochemical reduction of oxygen.

3.3. Circuit Analysis of the EIS Data

If EIS is to provide a technique to characterize changes or defects in the electrodes, an equivalent electronic circuit must be found to use as the "transform" to relate the EIS data to the electrode and electrolyte properties. We have previously investigated these relationships for larger activated iridium electrodes [10] and sputtered iridium oxide [11]. The current work seeks to extend the analysis to ultramicroelectrodes used for stimulation and to conditions more relevant to *in vivo* operation.

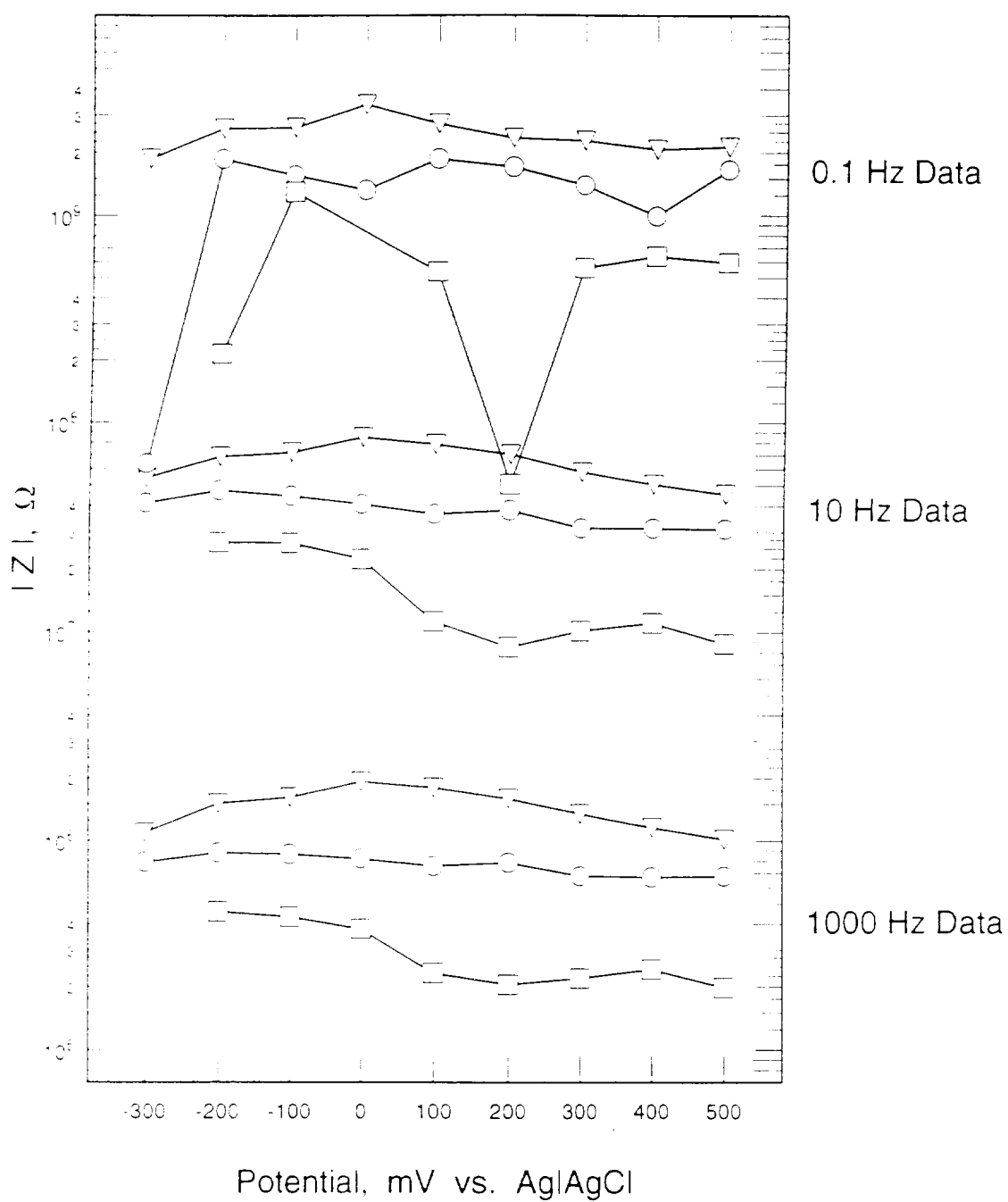
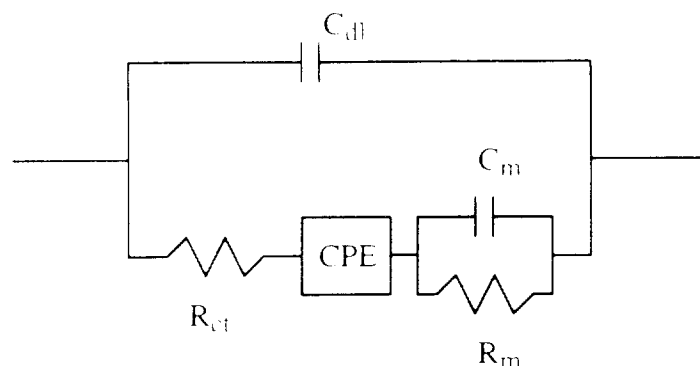


Figure 3.5 Comparison of the magnitude of the impedance as a function of electrode bias at three frequencies for the three EIS measurements. (∇) Site 2, Ribbon No. 4, least oxide, nondeaerated PBS. (\circ) Site 4, Ribbon No. 4, very thin oxide, deaerated PBS. (\square) Site 1, Ribbon No. 1, thin oxide, aerated PBS.



Scheme I

This quarter we began to evaluate different electronic circuits to fit the data in Figures 3.2 to 3.4. The initial circuit diagram was the one used previously for activated iridium [10] shown in Scheme I. Here C_{dl} is the double layer capacitance and R_{ct} is the reaction resistance. CPE is the constant phase element which is a frequency dependent impedance used in fitting the data. The C_m and R_m terms are a capacitance and resistance, respectively, associated with properties of the oxide film. Our first attempts to fit the data to this circuit have not led to values for the circuit elements that are physically significant. We are in the process, therefore, of modifying the circuit. We do not know as yet if these modifications are required because of the thin oxide layer, the small electrodes, the structure of the electrodes, or limitations of the instrumentation.

4. WORK FOR NEXT QUARTER

Additional ribbon-cable probe Ir microelectrodes will be tested to resolve the questions of the high background observed at high sweep rates in the Ru scan rate studies. Sites on the probes will be activated and EIS measured to determine the relationship between the impedance and the properties of the oxide films. This information will also help determine if there are any problems with the new formation techniques being used to make the electrode sites. We will also begin sputtering films of Ru/Ir alloys to determine if higher charge injection or improved electrode stability results from the activated alloys.

5. REFERENCES

1. Twardoch, U. M., private communication.
2. Mozota, J. and B. E. Conway, "Modification of Apparent Electrocatalysis for Anodic Chlorine Evolution on Electrochemically Conditions Oxide Films at Iridium Anodes," *J. Electrochem. Soc.*, vol. 128, pp. 2142-2149 (1981).
3. Mozota, J. and B. E. Conway, "Surface and bulk processes at oxidized iridium electrodes-I. Monolayer state and transition to reversible multilayer oxide film behaviour," *Electrochim. Acta*, vol. 28, pp. 1-8, 1983.
4. Twardoch, U. M. "Integrity of ultramicroelectrodes determined from electrochemical measurements," *J. Appl. Electrochem.*, vol. 24, pp. 835-857, 1994.
5. Aoki, K., K. Akimoto, K. Tokada, H. Matsuda, and J. Osteryoung, "Linear sweep voltammetry at very small stationary disk electrodes," *J. Electroanal. Chem.*, vol. 171, pp. 219-230, 1984.
6. Nicholson, R. S. and I. Shain, "Theory of stationary electrode polarography," *Anal. Chem.*, vol. 33, pp. 706-723, 1964.
7. Robblee, L. S., et al. "Studies of the Electrochemistry of Stimulating Electrodes," NINDS Contract No. N01-NS-1-2300, Quarterly Progress Report, No. 11, July 1991.
8. "Micromachined Stimulating Electrodes," NINDS Contract No. N01-NS-2-2379, Quarterly Progress Report, No. 9, February, 1995.
9. Boukamp, B. A., "Equivalent Circuit Users Manual" Report: CT88/265/128 and CT89-214-128, University of Twente, Department of Chemical Technology, May, 1989.
10. Aurian-Blajeni, B., X. Beebe, R. D. Rauh, and T. L. Rose, "Impedance of hydrated iridium oxide electrodes," *Electrochim. Acta*, vol. 34, pp. 795-802, 1989.
11. Aurian-Blajeni, B., M. M. Boucher, A. G. Kimball, and L. S. Robblee, "Physicochemical characterization of sputtered iridium oxide," *J. Mater. Res.*, vol. 4, pp. 440-446, 1989.